17. G. L. Bjoraker, H. P. Larson, V. G. Kunde, *Astrophys. J.* **311**, 1058 (1986).
18. B. E. Carlson, A. A. Lacis, W. B. Rossow, *J. Geophys. Res.* **99**, 14623 (1994).
19. M. Roos-Serote *et al.*, *J. Geophys. Res.* **103**, 23023 (1998).
20. P. G. J. Irwin *et al.*, *J. Geophys. Res.* **103**, 23001 (1998).
21. T. C. Owen *et al.*, *Eos* (Spring Suppl.) **77**, S171 (1996).
22. S. Atreya, M. H. Wong, T. Owen, H. Niemann, P. Mahaffy, in *Three Galileos: The Man, the Spacecraft, the Telescope* (proceedings of conference held 7 to 10 January 1997, Padova, Italy), J. Rahe, C. Barbieri, T. Johnson, A. Sohus, Eds. (Kluwer Academic, Dordrecht, Netherlands, 1997).
23. A. P. Showman and A. P. Ingersoll, *Icarus* **132**, 205 (1998).
24. R. D. Baker and G. Schubert, *Icarus* **136**, 340 (1998).
25. T. E. Dowling *et al.*, *Icarus* **132**, 221 (1998).
26. S. S. Limaye, *Icarus* **65**, 335 (1986).
27. The Brunt-Vaisala frequency, defined as the oscillation frequency for a vertically displaced air parcel, measures the atmosphere's static stability. On Earth and probably Jupiter, latent heat release in thunderstorms leads to a tropospheric temperature profile that decreases with height more slowly than the dry adiabatic profile and is hence stable to small-scale convection. For Jupiter, the dry adiabatic temperature gradient is –1.8 K km^{-1} whereas that with a Brunt-Vaisala frequency of 0.005 s^{-1} is –1.5 K km^{-1}.
28. We place the model bottom near 5 bars because latent heat effects are expected to generate a stable layer starting at about that altitude. The model assumes an ideal gas with a specific heat at constant pressure of 12,250 J kg^{-1} K^{-1} and gas constant of 3,500 J kg^{-1} K^{-1}. To verify that our results are independent of the boundary conditions, we performed some simulations with domains extending 360° in longitude or pole-to-pole in latitude.
29. The hyperviscosity is a high-order diffusion applied to all the dynamical variables and is typically ∇^4 for the first 30 Earth days of simulation and ∇^6 for subsequent times, with coefficients equal to half the upper limits from (*25*). The radiation is a Newtonian cooling that linearly relaxes temperature to an assumed equilibrium profile. The "sponge" is a Rayleigh drag, i.e., a linear relaxation of the winds to the assumed initial winds [from (*26*)], applied to the uppermost layers. These are all discussed extensively in (*25*).
30. The value of *a* is adjusted with the number of hot spots (generally 28°, 14°, 9°, and 6° longitude for 1, 2, 3, and 5 hot spots, respectively). The value of *b* is generally kept fixed at 4° latitude. We do not dynamically balance the winds inside the pressure anomalies. The model therefore undergoes a violent dynamical adjustment that lasts about 10 days. To prevent the adjustment phase from altering our results, we perform analysis only at times exceeding 50 days.
31. Hot spots are confined to 6° to 8°N latitude and have no counterpart in the southern hemisphere (*16*). Observations occasionally show equatorial plumes (10^4-km wedge-shaped clouds that are dynamically connected to hot spots) in the southern as well as northern hemisphere (*11*), however, suggesting that the confinement to a single hemisphere is not complete. Furthermore, ground-based observations before 1910 show plumes and dark features (presumably hot spots) in the southern rather than northern hemisphere, suggesting that long-period oscillations of hot spots between hemispheres may be possible.
32. Ground-based microwave observations show that ammonia is approximately 1 to 1.5 times solar from 2 to 5 bars over much of the planet (*7*). If NH_3 abundances of ~3 times solar are confined below 5 bars outside hot spots, then air parcels need only undergo pressure increases of twofold or less when entering hot spots to explain the probe ammonia observations, as opposed to the eightfold pressure increases indicated by comparison of equilibrium condensation models with probe data. To explain probe water measurements, however, the higher amplitudes may still be needed for parcels that enter hot spots deeper than 5 bars, unless (outside hot spots) water is confined to altitudes substantially below the condensation region in a manner analogous to that observed for ammonia.
33. R. F. Beebe, G. S. Orton, R. A. West, in *Time-Variable Phenomena in the Jovian System*, M. J. S. Belton, R. A. West, J. Rahe, Eds., NASA Spec. Publ. 494 (1989), pp. 245–288.
34. R. F. Beebe, A. A. Simon, L. F. Huber, *Science* **272**, 841 (1996).
35. A. J. Friedson and G. S. Orton, *Bull. Am. Astron. Soc.* **31**, 1155 (1999).
36. J. P. Boyd, in *Proceedings of the International School of Physics "Enrico Fermi" Course CIX: Nonlinear Topics in Ocean Physics* (North-Holland, New York, 1991), pp. 51–97.
37. A. R. Vasavada *et al.*, *Icarus* **135**, 265 (1998).
38. This research was supported by NASA and the NRC. We gratefully acknowledge numerous discussions with R. E. Young, J. Y-K. Cho, and A. P. Ingersoll.

20 April 2000; accepted 13 July 2000

Altered River Morphology in South Africa Related to the Permian-Triassic Extinction

Peter D. Ward,[1]* David R. Montgomery,[1] Roger Smith[2]

The Permian-Triassic transition in the Karoo Basin of South Africa was characterized by a rapid and apparently basin-wide change from meandering to braided river systems, as evidenced by preserved sedimentary facies. This radical changeover in river morphology is consistent with geomorphic consequences stemming from a rapid and major die-off of rooted plant life in the basin. Evidence from correlative nonmarine strata elsewhere in the world containing fluvial Permian-Triassic boundary sections suggests that a catastrophic terrestrial die-off of vegetation was a global event, producing a marked increase in sediment yield as well as contributing to the global $\delta^{13}C$ excursion across the Permian-Triassic boundary.

The Permian-Triassic (P-T) mass extinction killed more than 90% of marine species and about 70% of terrestrial vertebrate families (*1*). Several causes for the P-T extinction have been proposed, including an asteroid or comet impact (*2*), environmental change (*3, 4*), oceanic anoxia (*5*) or overturn (*6*), volcanism (*7, 8*), and synergistic combinations of these possible causes (*9*). Less is known about the extinctions on land than those in the sea. Perhaps the best studied record of vertebrate taxa across the P-T boundary is found in the Karoo Basin of South Africa, which records a complete stratigraphic record of Permian through Triassic systems in the interior of southern Pangaea and contains well-exposed P-T boundary sections with relatively abundant vertebrate fossils. The P-T boundaries in the Karoo can be correlated with marine P-T stratotypes using carbon isotope stratigraphy (*10*), which also indirectly dates the P-T boundary in the Karoo at about 251 million years ago (Ma) (*11*).

The record of vertebrate survivorship in the Karoo Basin is relatively well known. Only 6 of the 44 reptilian genera recovered to date from the highest Permian biostratigraphic zone (*Dicynodon* assemblage zone) are also found in the succeeding *Lystrosaurus* assemblage zone (*12*). The fossil record of Permian plants is less complete from the Karoo because of diagenesis, but correlative strata from other stratigraphic sections of Gondwanaland record a major floral extinction pulse at the boundary (*13*). The rapidity and cause of the extinctions among terrestrial organisms in the Karoo remains controversial, with claims of long-term (10^6 years) climate change (*14*) or more rapid (10^4 years) causes (*4*). In the latter study, the change of fluvial style, with concomitant changes in plant ecosystems, was suggested to be the cause of the vertebrate extinction in the basin. The proximal cause of this environmental change was thought to be a major pulse of tectonic activity along the southern margin of the Karoo, causing uplift in the basin (*4*).

We measured stratigraphic sections across seven P-T boundary localities scattered across 400 km of the Karoo Basin (*15*). These sections show similar changes in facies across the P-T boundary (Fig. 1). Three distinct facies associations were determined. Below the boundary, sandstone bodies show an association of sedimentary facies that are consistent with formation by scour and sedimentation in a confined unidirectional flow, such as is produced by large meandering rivers of high sinuosity. These meandering channel sandstones are commonly single-storied and are characterized by low-angle (20° to 25°) lateral accretion surfaces that extend throughout the thickness of the channel sandstone and into the overlying channel bank deposits as interdigitating sandstone string-

[1]Department of Geological Sciences, University of Washington, Seattle, WA 98195, USA. [2]South African Museum, Cape Town, South Africa.

*To whom correspondence should be addressed.

ers. The lower portion of the accretion unit is made up of predominantly trough cross-bedded and horizontally laminated fine-grained sandstone with some clay pebble conglomerate at the base. The upper parts of the point bar sandstones are ripple cross-laminated and commonly display mudstone-draped rippled surfaces. These sands are interbedded with olive gray mudstone.

The second facies assemblage is associated with the boundary itself, as recognized by the last occurrence of the dicynodont genus *Dicynodon* as well as a negative excursion in $\delta^{13}C$. The boundary is within a laminated sandstone-shale unit several meters thick that is uniquely found at this interval. The laminated beds are under and overlain by sheet sandstone bodies ranging from 1 to 5 m thick with some conglomerate-lined internal discontinuities and basal contacts that are characteristically "gullied," as opposed to having the wide, shallow scoured bases of the underlying sandstones of the previously described facies. The gullied bases are often filled with conglomerate lags.

The third facies association is found in the lowermost Triassic parts of the *Lystrosaurus* zone and is characterized by a suite of sedimentary facies typically formed by braided river systems. These facies contain a higher proportion of sandstone to shale than in the underlying Permian, and, in contrast to the Permian-aged sandstone bodies beneath, are multistoried and vertically accreted. Each story (5 to 10 m thick) comprises an erosively based tabular sandstone, horizontally laminated, with numerous irregular patches of maroon mudrock clasts. Uneroded tops of these sandstone units display dune forms structured by planar cross-bedding with plane-parallel laminations. Scour surfaces of these sandstones are draped with mudstone pebble conglomerate. Interchannel sequences are coarser than the underlying mud units of the *Dicynodon* zone, which we interpret as being indicative of higher sedimentation rates. These sandstone units also lack the inclined lateral accretion surfaces of the Permian sandstone of the underlying facies, and are thus similar to sands forming in modern-day braided river systems. The subordinate interchannel silt and mudstone facies are predominantly maroon in color, in contrast to the olive colors of the Permian.

The change in facies described above occurs over 30 m or less of section (and over as little as 10 m in some sections). We interpret these facies changes to have occurred because of a change of river sinuosity from high to low.

A change from meandering to braided river patterns can be triggered by a number of causes. At a given discharge, braided channels occur on steeper slopes than do meandering channels (*16*). On the basis of this relation, a change from meandering to braided morphology can be inferred to reflect an increased channel slope, as earlier posited for the Karoo Basin (*4*). However, during the

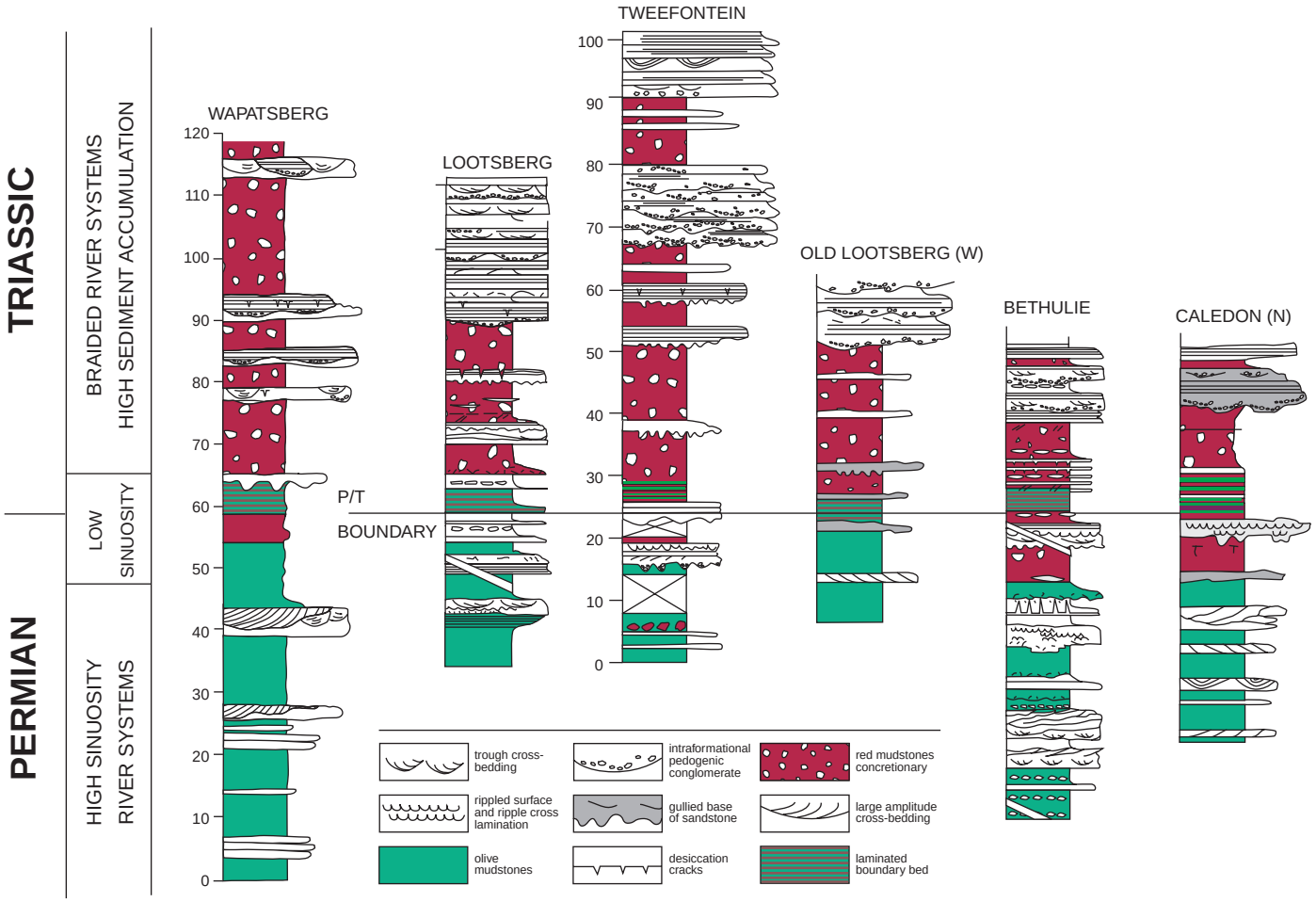

Fig. 1. Karoo Basin measured stratigraphic sections used in this study, showing change in sedimentary facies across the P-T boundary interval that we interpret as being caused by a changeover from high-sinuosity river systems to braided river systems. GPS for localities as follows: Wapatsberg S31, 54.879; W24, 53.794. Lootsberg S31, 51.005; W24, 52.299. Tweefontein S31, 49.334; W24, 48.565. Old Lootsberg (W) S31, 47.600; W24, 47.754. Bethulie S30, 24.989; W26, 17.234. Caledon (N) S30, 26.675; W26, 18.006. The P-T boundary is defined by the last occurrence of *Dicynodon* sp. at the Lootsberg, Old Lootsberg, Bethulie, and Caledon sections, and by the presence of a significant isotopic anomaly at Bethulie and Lootsberg. The environmental effect causing both the extinction and the isotopic perturbation probably occurred earlier and may coincide with the changeover from high-sinuosity to low-sinuosity river systems, as interpreted from a change in sedimentary facies in the six sections.

P-T interval there is no record of major orogenic events in the basin that could have resulted in the striking sedimentological changeover from meandering to braided river systems. Deformation of the Karoo is well dated, with major episodes of folding and uplift occurring for approximately million-year intervals at about 258 and 247 Ma (*17*). The recent dating of the P-T boundary at 250 Ma (*8*), rather than 247 Ma as long believed, invalidates the hypothesis that the change in sedimentary facies across the P-T boundary in the Karoo was triggered by a pulse in tectonic activity.

An alternative hypothesis is that the changeover from high-sinuosity to low-sinuosity channel morphology was brought about by a major plant die-off, because sediment loading and the nature of channel bank vegetation also influence the development of braided channel morphology. High rates of bedload transport can cause braiding, and loss of cohesive channel-margin vegetation can convert a meandering channel to a braided morphology (*18*). Consequently, a stratigraphic change from a meandering to a braided channel could be due to increased sediment loading or loss of channel-margin vegetation. Numerical models of sediment transport processes (*19*) show that the essential factors necessary for development of braided channels are high rates of bedload transport and flow unconstrained by cohesive or resistant banks. Field experiments on channel bank scour (*20*) show that banks protected by a root mat had erosion resistances several orders of magnitude greater than that of comparable bank sediment without vegetation. Hence, a die-off of flood plain vegetation would favor the development of braided channels because of the decreased strength of channel banks.

A basin-wide die-off of vegetation would also increase sediment delivery from hill slopes, and thereby would increase sediment loads in channels. Vegetation provides substantial erosion resistance, and hill slope sediment yields are sensitive to changes in vegetation abundance, composition, and health, with decreased vegetation cover leading to greater erosion (*21*). Documented cases of high sediment yields after watershed-wide vegetation disturbance include forest fires (*22*), land use change and agricultural practices (*23*), and volcanic eruptions (*24*). Field studies also show that increased sediment supply from watershed disturbance or large local sediment sources can lead to channel braiding (*25*). Hence, lacking independent evidence for tectonic forcing at the right time, we propose that the observed transition from meandering to braided channels in the ancient Karoo Basin is better explained by increased sediment delivery from vegetation-denuded hill slopes to channels lacking abundant rooted plants on their flood plain.

If our hypothesis for the Karoo Basin is applicable on a global scale, then we would expect to see a similar response to increased sediment loading—such as a change from meandering to braided channels—for other fluvial basins that span the P-T boundary. It has been speculated that braided channels were the dominant fluvial morphology before the evolution of vegetation, and that meandering channels only became prevalent after the evolution of primitive terrestrial vegetation (*26*). Cotter's (*27*) compilation of paleochannel patterns indicates that almost all reported pre-Silurian fluvial deposits have been interpreted as braided systems. Subsequent reviews have confirmed that Proterozoic fluvial deposits were formed by braided river systems (*28*). Plotted as a time series, Cotter's data show that the proportion of channels interpreted as braided increased from the Permian to the Triassic and then subsequently decreased.

Local as well as global compilations support this view. Of the 14 P-T fluvial basins studied to date in Europe (*29*), only 3 basins had complete boundary sequences. Two of these basins had fluvial braid plains on both sides of the P-T boundary; because these channels were already braided in the Permian, they are not a relevant test of our hypothesis. In contrast, the P-T boundary in the South Devon Basin occurs between the Upper Permian Littleham mudstones, interpreted to be a fluvial flood plain environment, and the Lower Triassic Budleigh Salterton Pebble Beds, interpreted to be a fluvial braid plain—a transition similar to that in the Karoo Basin. Distinctive claystone breccias at the P-T boundary in the fluvial stratigraphy of the Sydney Basin, Australia, have been interpreted (*3, 30*) as reflecting a pulse of intense soil erosion. In every boundary sequence examined in this study, faster sediment accumulation rates were observed in the earliest Triassic than in the latest Permian strata. The global hiatus in coal formation at the P-T boundary is consistent with increased watershed sediment yields as well as extinction of the peat-forming flora (*3*).

We thus interpret the short-term dominance of braided over meandering river facies in Triassic rocks as a consequence of the P-T extinction, and we predict that Lower Triassic strata will show more rapid sedimentation rates than uppermost Permian units.

Independent evidence for a sediment yield pulse at the P-T boundary is present in abrupt changes in ^{13}C and ^{18}O across the P-T boundary (*31*). Inorganic as well as organic oceanic $\delta^{13}C$ changed across the P-T boundary, but fractionation of $\delta^{13}C$ between carbonate and organic matter remained constant. This result indicates an increased delivery of terrestrial carbon to reservoirs in shallow and deep oceanic environments and reduced primary productivity after the P-T mass extinction. These records indicate that it took 50,000 to 100,000 years after the P-T boundary for $\delta^{13}C$ values to recover, a time scale similar to that interpreted for the period of dominantly braided channel morphology in the Karoo Basin (*6*). Examination of isotopic data (*31*) shows that the recovery followed an approximately exponential pattern. An exponential decay of sediment yield is expected after watershed disturbance (*32*), and 50,000 to 100,000 years is a reasonable time scale over which to expect such change to occur.

We have no explanation for what caused the P-T extinction event, but the evidence presented above is consistent with the interpretation that major sedimentary changes in fluvial environments associated with the P-T event are due to die-off of land plants. Our results confirm that the facies transition across the P-T boundary from meandering to braided river systems is nearly basin-wide (and potentially a global phenomenon). The global increase in the prevalence of braided facies patterns in the earliest Triassic suggests a return of most fluvial environments to a character typical of the period before the evolution of land plants. The increased sediment yield that would have resulted from a basin-wide change in vegetation sufficient to trigger such widespread and sustained fluvial response would have drastically increased terrestrial exports of organic and inorganic sediment (and therefore ^{13}C) to the oceans, and may have contributed to the loss of shallow-water marine taxa across P-T boundary sections. The P-T extinction may well have begun on land immediately before its inception in the ocean, thus contributing in some manner to the marine phase of the extinction.

References and Notes

1. D. H. Erwin, *Nature* **367**, 231 (1994).
2. M. R. Rampino and B. M. Haggerty, *Hazards Due to Asteroids* (Univ. of Arizona Press, Tucson, AZ, 1996), p. 827.
3. G. J. Retallack, *Geol. Soc. Am. Bull.* **111**, 52 (1999); J. N. Thackeray *et al*., *Nature* **347**, 751 (1990); S. Stanley and X. Yang, *Science* **266**, 1340 (1994).
4. R. M. Smith, *Palaeogeogr. Palaeoclimatol. Palaeoecol.* **117**, 81 (1995).
5. P. B. Wignall and R. J. Twitchett, *Science* **272**, 1155 (1996); Y. Isozaki, *Science* **276**, 235 (1997).
6. A. H. Knoll, R. K. Bambach, D. E. Canfield, J. P. Grotzinger, *Science* **273**, 452 (1996).
7. I. H. Campbell, G. K. Czamanske, V. A. Fedorenko, R. I. Hill, V. Stepanov, *Science* **258**, 1760 (1992).
8. P. R. Renne, Z. Zichao, M. A. Richards, M. T. Black, A. R. Basu, *Science* **269**, 1413 (1995).
9. D. H. Erwin, *The Great Paleozoic Crisis* (Columbia Univ. Press, New York, 1993); R. Morante, *Hist. Biol.* **11**, 289 (1996).
10. K. G. MacLeod, R. Smith, P. Koch, P. D. Ward, *Geology* **28**, 227 (2000).
11. S. A. Bowring *et al*., *Science* **280**, 1039 (1998).
12. B. Rubidge, *Geol. Surv. S. Afr. Biostratigraphy* (1995), p. 1.
13. J. M. Anderson *et al*., *J. Afr. Earth Sci.* **28**, 145 (1999); H. Visscher *et al*., *Proc. Natl. Acad. Sci. U.S.A.* **93**, 2135 (1996).
14. G. M. King, *Palaeontol. Afr.* **27**, 31 (1990).
15. Stratigraphic sections were measured during September 1997, September to November 1998, and Octo-

ber 1999 in the Lootsberg Pass region and around the town of Bethulie using Jacobs staff. Interpretations of sedimentary facies were made in the field and transferred to the measured sections. Fossil material was collected at that time by the authors and by members of the South African Museum field teams. Stratigraphic sections include those of Lootsberg Pass, Old Lootsberg Pass, Wapatsberg Pass, Tweefontein, Bethulie, and Twin Rivers game park. Data on the occurrence of fluvial facies types from Precambrian river systems were derived from literature sources.

16. L. B. Leopold and M. G. Wolman, *U.S. Geol. Surv. Pap. 282-B* (1957).
17. J. J. Veevers, D. L. Cole, E. J. Cowan, *Geol. Soc. Am. Mem.* **184**, 223 (1994); O. Catuneanu, P. J. Hancox, B. S. Rubidge, *Basin Res.* **10**, 417 (1998).
18. S. A. Schumm, *Annu. Rev. Earth Planet. Sci.* **13**, 5 (1985).
19. A. B. Murray and C. Paola, *Earth Surf. Processes Landforms* **22**, 1001 (1997); *Nature* **371**, 54 (1994).
20. D. G. Smith, *Geol. Soc. Am. Bull.* **87**, 857 (1976).
21. I. P. Prosser and C. J. Slade, *Geology* **22**, 1127 (1994); I. P. Prosser and W. E. Dietrich, *Water Resources Res.* **31**, 2867 (1995).
22. R. S. Sartz, *J. Soil Water Conserv.* **8**, 279 (1953); J. A. Krames, *Dept. Agric. Misc. Publ. 970* (1965), p. 85; K. M. Scott, *U.S. Geol. Surv. Prof. Pap. 750-C* (1971), p. 242; L. E. Jackson, *U.S. Geol. Surv. J. Res.* **5**, 17 (1977); K. M. Scott and G. P. Williams, *U.S. Geol. Surv. Prof. Pap. 1030* (1978).
23. S. J. Ursic and F. E. Dendy, in *Proceedings of the Federal Inter-Agency Sedimentation Conference* (1965); T. Dunne, *J. Hydrol.* **42**, 281 (1979).
24. H. Kadomura, T. Imagawa, Y. Hiroshi, *Z. Geomorphol. Suppl.* **46**, 124 (1983); B. D. Collins and T. Dunne, *Geol. Soc. Am. Bull.* **97**, 986 (1986); S. K. Hayes, thesis, University of Washington, Seattle (1999).
25. N. D. Smith and D. G. Smith, *Geology* **12**, 78 (1984); A. M. Harvey, *Earth Surf. Processes Landforms* **16**, 675 (1991).
26. S. A. Schumm, *Geol. Soc. Am. Bull.* **79**, 1573 (1968).
27. E. Cotter, *Can. Soc. Petrol. Geol. Mem.* **5**, 361 (1978).
28. P. G. Eriksson *et al.*, *Sediment. Geol.* **120**, 5 (1998).
29. D. Mader, *Evolution of Palaeoecology and Palaeoenvironment of Permian and Triassic Fluvial Basins in Europe* (Fischer, Stuttgart, 1992), vol. 1.
30. G. J. Retallack and E. S. Krull, *Aust. J. Earth Sci.* **46**, 785 (1999).
31. M. Magaritz, R. V. Krishnamurthy, W. T. Holser, *Am. J. Sci.* **292**, 727 (1992); K. Wang, H. H. Geldsetzer, H. R. Krouse, *Geology* **22**, 580 (1994).
32. S. A. Schumm and D. K. Rea, *Geology* **23**, 391 (1995).
33. Supported by NSF grant EAR 9903382 (P.D.W.).

24 May 2000; accepted 10 July 2000

Historical Trends in Lake and River Ice Cover in the Northern Hemisphere

John J. Magnuson,[1]* Dale M. Robertson,[2] Barbara J. Benson,[1] Randolph H. Wynne,[3] David M. Livingstone,[4] Tadashi Arai,[5] Raymond A. Assel,[6] Roger G. Barry,[7] Virginia Card,[8] Esko Kuusisto,[9] Nick G. Granin,[10] Terry D. Prowse,[11] Kenton M. Stewart,[12] Valery S. Vuglinski[13]

Freeze and breakup dates of ice on lakes and rivers provide consistent evidence of later freezing and earlier breakup around the Northern Hemisphere from 1846 to 1995. Over these 150 years, changes in freeze dates averaged 5.8 days per 100 years later, and changes in breakup dates averaged 6.5 days per 100 years earlier; these translate to increasing air temperatures of about 1.2°C per 100 years. Interannual variability in both freeze and breakup dates has increased since 1950. A few longer time series reveal reduced ice cover (a warming trend) beginning as early as the 16th century, with increasing rates of change after about 1850.

Calendar dates of freezing and thawing of lakes and rivers were being recorded by direct human observation well before scientists began to measure, manipulate, and model these freshwater ecosystems (*1*). The early observations were made for religious and cultural reasons (*2, 3*), for practical reasons concerned with transportation over ice or open water (*4*), and, apparently, simply out of curiosity. These simple records provide a seasonally integrated view of global warming from regions where early temperature measurements are sparse.

Here, we present and analyze the trends from time series that are longer than 100 years on lakes and rivers around the Northern Hemisphere. Thirty-nine time series are available for the 150-year period from 1846 to 1995 (*5*); three sites from Russia, Finland, and Japan with records beginning before 1800 are also available. The "freeze date" is defined as the first date on which the water body was observed to be totally ice covered, and the "breakup date" is the date of the last breakup observed before the summer open-water phase (*6*).

Between 1846 and 1995, 38 of 39 records change in the direction of later freeze dates (14 of 15) and earlier breakup dates (24 of 24) (Fig. 1 and Table 1) (*7*). The single exception, Lake Suwa, Japan, freeze dates, was not significant ($P = 0.25$). Individual slopes (9 out of 15 for the freeze date and 16 out of 24 for the breakup date) were statistically significant ($P < 0.05$). Linear trends over the 150 years averaged a freeze date that was 5.8 days/100 years later (±1.9 days, confidence interval 95%) and a breakup date that was 6.5 days/100 years earlier (±1.4 days, confidence interval 95%).

Slopes did not differ statistically between freeze and breakup dates (matched pair *t* test; $n = 12$; $P = 0.37$), among latitudes, between North America and Eurasia, nor between rivers (7.8 days/100 years) and lakes (5.9 days/100 years) (*t* test; $n = 7, 30$; $P > 0.25$). The overall rate of change for the Northern Hemisphere has been 6.2 days/100 years between 1846 and 1995, including all records except Toronto Harbor (Table 1) and giving equal weight to freeze and breakup.

The few records before 1846 suggest that long-term changes toward later freezing and earlier breakup dates were already occurring, but at slower rates, at sites as far apart as Europe and Japan. Three time series (one lake and two rivers) have records that are long enough to provide annual information on ice phenology trends before 1846 (Fig. 2 and Table 1).

For Lake Suwa, Japan, freeze dates became later over the 550-year record by 2.0 days/100 years ($P < 0.0001$) (Fig. 2). Slopes indicating later freezing for relatively unbroken windows of time ranged from 3.2 days/100 years (1443 to 1592) to 20.5 days/100 years (1897 to 1993). Additional evidence from Lake Suwa comes from the ice cover occurrence data. Lake Suwa was ice covered for 240 out of 243 winters (99%) from 1443 to 1700 but only for 261 out of 291 winters

[1]Center for Limnology, University of Wisconsin–Madison, Madison, WI 53706, USA. [2]U.S. Geological Survey, Water Resources Division, 8505 Research Way, Middleton, WI 53562, USA. [3]Department of Forestry, Virginia Polytechnic Institute and State University, 319 Cheatham Hall, Blacksburg, VA 24061, USA. [4]Department of Environmental Physics, Swiss Federal Institute of Environmental Science and Technology, Überlandstrasse 133, CH-8600 Dübendorf, Switzerland. [5]Department of Geography, Rissho University 4-2-16 Osaki, Shinagawa-Ku, Tokyo 141, Japan. [6]Great Lakes Ecosystem Research Laboratory, National Oceanic and Atmospheric Agency, 2205 Commonwealth Boulevard, Ann Arbor, MI 48105–1593, USA. [7]World Data Center for Glaciology, University of Colorado at Boulder, Boulder, CO 80309–0449, USA. [8]College of Arts and Sciences, Metropolitan State University, 700 East 7 Street, St. Paul, MN 55106, USA. [9]Finnish Environment Institute, Post Office Box 140, FIN-00251 Helsinki, Finland. [10]Limnological Institute, Post Office Box 4199, Irkutsk 664033, Russia. [11]National Water Research Institute, Environment Canada, 11 Innovation Boulevard, Saskatoon, SK S7N 3H5, Canada. [12]Department of Biological Science, State University of New York at Buffalo, Buffalo, NY 14260, USA. [13]State Hydrological Institute, 23 Second Line, St. Petersburg 199053, Russia.

*To whom correspondence should be addressed. E-mail: jmagnuson@mhub.limnology.wisc.edu